Multistimuli-Responsive Supramolecular Vesicles Based on Water-Soluble Pillar[6]arene and SAINT Complexation for Controllable Drug Release

Yu Cao,[†,‖] Xiao-Yu Hu,[†,‖] Yan Li,[‡] Xiaochun Zou,[†,§] Shuhan Xiong,[†] Chen Lin,[†] Ying-Zhong Shen,[§] and Leyong Wang*,[†]

[†]Key Laboratory of Mesoscopic Chemistry of MOE, Center for Multimolecular Organic Chemistry, School of Chemistry and Chemical Engineering, Nanjing University, Nanjing 210093, China

[‡]State Key Laboratory of Bioelectronics and Jiangsu Key Laboratory of Biomaterials and Devices, School of Biological Science and Medical Engineering, Southeast University, Nanjing 210009, China

[§]College of Material Science and Technology, Nanjing University of Aeronautics and Astronautics, Nanjing 210016, China

Ⓢ Supporting Information

ABSTRACT: Supramolecular binary vesicles based on the host−guest complexation of water-soluble pillar[6]arene (**WP6**) and SAINT molecule have been successfully constructed, which showed pH-, Ca^{2+}-, and thermal-responsiveness. These supramolecular vesicles can efficiently encapsulate model substrate calcein, which then can be efficiently released either by adjusting the solution pH to acidic condition due to the complete disruption of vesicular structure, or particularly, by adding a certain amount of Ca^{2+} due to the Ca^{2+}-induced vesicle fusion and accompanied by the structure disruption. More importantly, drug loading and releasing experiments demonstrate that an anticancer drug, DOX, can be successfully encapsulated by the supramolecular vesicles, and the resulting DOX-loaded vesicles exhibit efficient release of the encapsulated DOX with the pH adjustment or the introduction of Ca^{2+}. Cytotoxicity experiments suggest that the resulting DOX-loaded supramolecular vesicles exhibit comparable therapeutic effect for cancer cells as free DOX and the remarkably reduced damage for normal cells as well. The present multistimuli-responsive supramolecular vesicles have great potential applications in the field of controlled drug delivery. In addition, giant supramolecular vesicles (~3 μm) with large internal volume and good stability can be achieved by increasing the temperature of **WP6** ⊃ SAINT vesicular solution, and they might have potential applications for bioimaging.
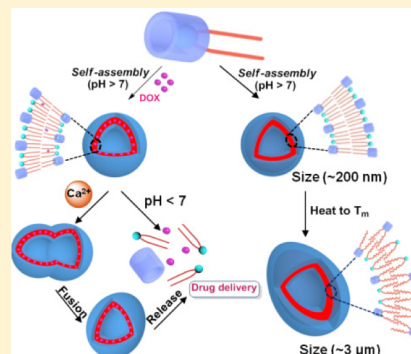
INTRODUCTION

One of the main challenges in current supramolecular chemistry is how to narrow the gap between the general principles of molecular recognition/self-assembly and their applications in biology and medical materials. Construction of vesicles with desired shape, size, and properties endow them special functions for the development of biomimetic systems, drug/gene delivery systems, and microreactors.[1] Recently, studies on stimuli-responsive supramolecular vesicles[2] have become an extraordinarily fascinating topic, due to their unique structures that can efficiently encapsulate drugs, shield them from degradation, reduce their cytotoxicity, and release them with specific external stimulus. Up to now, various strategies for the construction of single stimulus-responsive supramolecular vesicles that are responsive to photo-,[2b,g] electro-,[2i] thermo-,[2c] pH-,[2d,e,h−j] enzyme-[2a] or chemostimuli,[2k] respectively, have been exploited; however, there are only a few reports on the construction of multistimuli-responsive supramolecular vesicles based on noncovalent interactions.[3] Therefore, the fabrication of multistimuli-responsive supramolecular vesicles constructed by supramolecular amphiphiles through noncovalent inter-

actions is of great interest and importance for their applications in the field of biotechnology and biomedicine, particularly of drug delivery.

So far, although several kinds of noncovalent interactions have been used to fabricate supramolecular amphiphiles, supramolecular vesicles constructed by supramolecular amphiphiles, particularly by pillararene-based supramolecular amphiphiles, have been much less frequently explored in the field of drug delivery.[2a,d,4] Water-soluble pillararenes (**WP6**)[2f,5] have been demonstrated to be significantly biocompatible in aqueous media (Scheme 1),[2d,e] which is of importance for their applications in drug delivery. SAINT molecules[6] which are pyridinium amphiphiles with one pyridinium group and two alkyl chains have been widely applied for the delivery of DNA into cells as highly efficient vectors,[1a,7] but the characteristic of SAINT as cationic nanocarriers has greatly limited their applications in biology and drug delivery due to the blood clotting caused by the cation effect. Since the host−guest

Scheme 1. Schematic Illustration of the Formation of Multistimuli-Responsive Supramolecular Vesicles
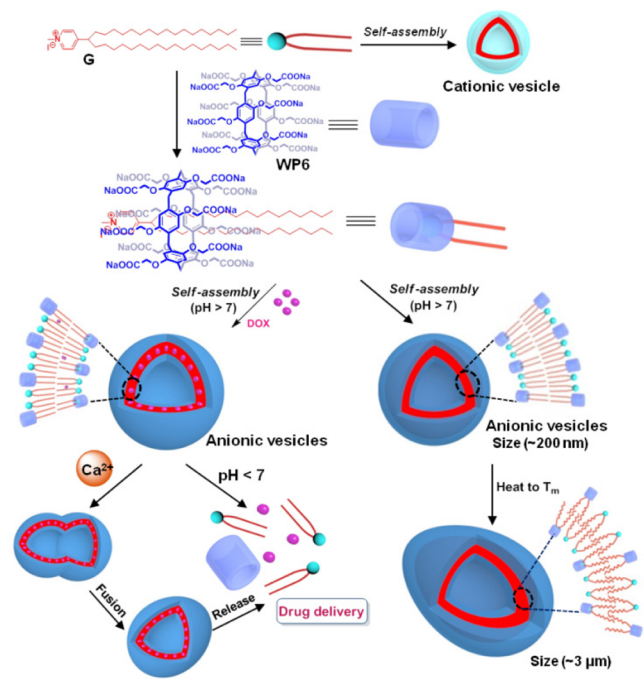
recognition motif based on **WP6** and pyridinium salt has been demonstrated to have a strong binding affinity in water driven by hydrophobic and electrostatic interactions,[2f] we envision that the supramolecular amphiphile could be achieved from **WP6** and SAINT derivatives based on the host−guest interaction of **WP6** and the pyridinium moiety of SAINT (Scheme 1). Moreover, the charges of the original cationic SAINT derivatives would be converted to anionic **WP6** ⊃ SAINT complex, and the obtained supramolecular amphiphile would be possibly able to form anionic supramolecular vesicles in water by self-assembly, which would eliminate the limitation of cationic SAINT derivatives for the applications in drug delivery.

Following our previous work that pillararene-based single pH-responsive supramolecular vesicles were first applied as drug delivery system for intracellular drug delivery,[2d] herein, we report the successful construction of a novel type of multistimuli-responsive nanoscale pillararene-based supramolecular binary vesicles from **WP6** and SAINT molecule **G** (Scheme 1), which are demonstrated to be efficient carriers for encapsulation and controlled release of anticancer drug doxorubicin (DOX) by either adjusting the solution pH or introducing Ca^{2+}. Particularly, it is found that the addition of Ca^{2+} could induce rapid fusion of **WP6** ⊃ **G** vesicles accompanied by the structure disruption, achieving Ca^{2+}-responsiveness. In the last few decades, the research on the Ca^{2+}-induced real-time cytomimetic fusion process of lipid vesicles (liposomes) and polymeric vesicles has been reported.[8] However, it is the first time to observe the Ca^{2+}-induced fusion process of supramolecular vesicles, which provides the useful information for understanding the fusion process concerning with supramolecular interactions. Since Ca^{2+} plays essential roles in a number of biochemical processes and the aberrations of calcium concentration in the plasma have been associated with many diseases, such as cancer,[9] as an appealing exploration for therapeutic purposes, the drug-loaded supramolecular

vesicles with Ca^{2+}-responsiveness may find potential applications in the field of biotechnology, diagnostics, and drug delivery systems (DDS). The cytotoxicity experiments demonstrate that the resulting DOX-loaded supramolecular vesicles exhibit comparable therapeutic effect for cancer cells as free DOX and the remarkably reduced damage for normal cells. In addition, giant supramolecular vesicles with large internal volume and good stability can be achieved from small supramolecular vesicles formed from **WP6** and SAINT by increasing the temperature of the vesicular solution,[6c,10] exhibiting the thermal-responsiveness, which might have the potential applications for bioimaging.

■ RESULTS AND DISCUSSION

Host−Guest Complexation Study. **WP6**, SAINT molecule **G**, and model compound **G**′ were synthesized according to established procedures.[2f,7c,10b] Initially, the complexation between **WP6** and guest **G** would be investigated by ^{1}H NMR spectroscopy, but the clear ^{1}H NMR spectrum of **G** could not be possibly obtained due to its poor solubility in aqueous solution. Therefore, the model compound **G**′ (1-methyl-4-(pentan-3-yl)pyridin-1-ium iodide, an analogue of **G**) was used for the host−guest complexation study of **WP6** and **G**. Figure 1 showed the ^{1}H NMR titration results of **WP6** that
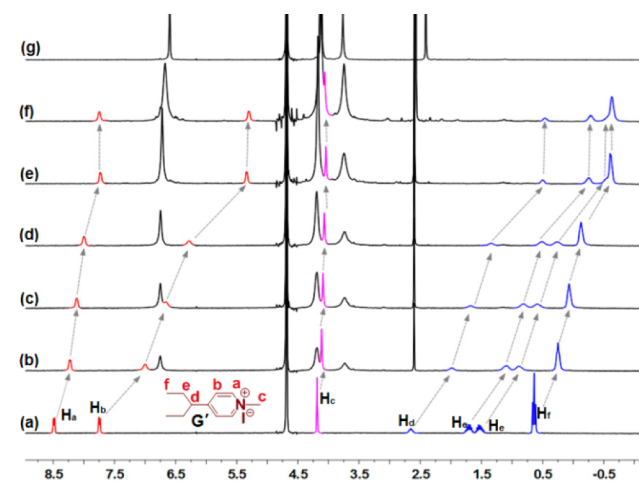
Figure 1. ^{1}H NMR spectra (300 MHz, D_2O, 298 K) of **G**′ at a constant concentration of 2 mM with different concentrations of **WP6**: (a) 0.00, (b) 1.00, (c) 1.33, (d) 2.00, (e) 4.00, (f) 6.00 mM, and (g) only **WP6** (5 mM).

was added into a solution of **G**′ in D_2O, from which remarkable upfield chemical shifts of the pyridine protons (H_a and H_b), methenyl, methylene, and methyl protons (H_d, H_e, and H_f) of **G**′ were observed upon addition of **WP6** due to the shielding effect of the electron-rich cavities of **WP6** toward **G**′, while no obvious change was observed for the N-methyl protons (H_c) of **G**′. The above results revealed that guest **G**′ threaded into the host **WP6** with its protons H_a, H_b, H_d, H_e, and H_f in the hydrophobic **WP6** cavity and N-methyl protons H_c out of the cavity. Moreover, 2D NOESY experiment was also performed to investigate the spatial conformation of such inclusion complex (Figure S2, Supporting Information), from which NOE correlation signals were observed between protons H_1 of **WP6** and H_b, H_e, H_f of **G**′, as well as protons H_3 of **WP6** and H_e, H_f of **G**′, confirming the above threading binding mode.

10763

dx.doi.org/10.1021/ja505344t | J. Am. Chem. Soc. 2014, 136, 10762−10769

Subsequently, ITC experiment, which is a powerful tool for investigating the host−guest complex interactions, was applied to determine the binding constant (K_a) and the thermodynamic parameters (enthalpy and entropy changes $\Delta H°$ and $\Delta S°$) of **WP6** ⊃ **G'** complex.[11] On the basis of the ITC data (Figure S5, Supporting Information), K_a for the formation of 1:1 **WP6** ⊃ **G'** complex was calculated to be (1.67 ± 0.13) × 10^5 M^{-1} with a good "*N*" value of 1.09 by the curve fitting. Moreover, from the ITC data, the 1:1 complexation between **WP6** and **G'** could be obtained, which was driven by a favorable enthalpy change ($\Delta H°$ = −11.74 kJ·mol^{-1}), accompanied by positive entropy change ($T\Delta S°$ = 18.09 kJ·mol^{-1}). In addition, the 1:1 stoichiometry complex between **WP6** and the real guest **G** was also confirmed by Job's plot method using the UV−vis spectroscopy (Figure S1, Supporting Information).

Construction of Supramolecular Binary Vesicles Based on the Host−Guest Complexation of WP6 with SAINT (G).

After the accomplishment of the amphiphilic **WP6** ⊃ **G** recognition motif in water, the ability of the above supramolecular complex to form higher-order aggregates in water was further investigated. Because of the poor solubility of **G** in water, we rapidly injected **G** (0.014 mmol, dissolved in 4 mL of ethanol) into 95 mL of deionized (DI) water, and then another portion of DI water was filled until the volume of the solution reached 100 mL. This resulting solution was investigated by transmission electron microscopy (TEM), dynamic laser scattering (DLS), and UV−vis experiments, which showed that no aggregate assembled by **G** itself existed under examined conditions although the guest **G** itself is an amphiphilic molecule and it was reported to be able to form vesicle structure in aqueous soltuion.[6c] However, with the addition of **WP6**, a light blue opalescence was obviously observed form the aqueous solution. The size and morphology of this nanostructural aggregates formed by **WP6** ⊃ **G** supramolecular amphiphile in aqueous solution are shown in Figure 2 by DLS and TEM, respectively. DLS result showed
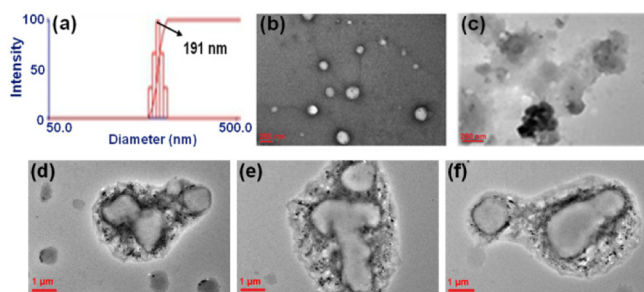
Figure 2. (a) DLS data of the **WP6** + **G** vesicles. TEM images: (b) **WP6** + **G** vesicles; (c) **WP6** + **G** vesicles after the solution pH was adjusted to 5.0; (d−f) **WP6** + **G** vesicles after the addition of calcium chloride (5.0 mM), and then quenching with EDTA after 5 min.

that the **WP6** ⊃ **G** complex formed aggregates with a narrow size distribution, giving an average diameter of 191 nm (Figure 2a), and TEM images indicated the hollow spherical morphology with a diameter ranging from 120 to 200 nm, convincingly indicating the formation of suprmolecular vesicular structure (Figure 2b).

Since it was observed that the addition of different amount of **WP6** led to obvious changes of opalescence intensity in aqueous solution, it is necessary to determine the best molar fraction of **WP6** and **G** to form aggregates, which was then

determined by the UV−vis titration experiments (Figure S3, Supporting Information). Upon gradually increasing the amount of **WP6** that was added, it was found that the absorbance evolution at 350 nm underwent a sharp increase thereafter an inverse decrease upon further addition of **WP6**. This rapid increase of the absorbance intensity indicated that **WP6** and **G** formed a higher-order complex with a tendency toward amphiphilic aggregation, whereas it underwent disassembly upon further addition of **WP6**, generating a simple 1:1 supramolecular inclusion complex. Thus, the best molar ratio 12:1 (**G**/**WP6**) for the formation of supramolecular amphiphilic vesicles was determined at the inflection point (Figure S3b, Supporting Information). Moreover, ζ-potential,[12] which is also called the electric potential, refers to the potential at the shear plane, was applied for investigating the stability of the obtained vesicles. It was found that the ζ-potential of the vesicles gradually changed from positive (+30 mV, [**G**]/[**WP6**] = 40:1) to negative (−30 mV, [**G**]/[**WP6**] = 7:1) upon addition of **WP6** in the titration experiments (Figure S4, Supporting Information). In particular, the ζ-potential of the vesicles formed at the best molar fraction ([**G**]/[**WP6**] = 12:1) was close to 0 mV, which means that vesicles obtained at the best molar ratio were not stable. Therefore, considering the repulsive-force-induced increasing-stability of vesicles, the molar ratio of 10:1 [**G**]/[**WP6**] (ζ-potential = −25 mV) was chosen for further investigation of their stimuli-responsive behavior as well as their applications in drug delivery.

Multistimuli-Responsiveness of the Supramolecular Vesicles.

The supramolecular vesicles with multistimuli-responsiveness are of extreme importance to their applications in DDS. Tyndall effect of the **WP6** ⊃ **G** ([**G**]/[**WP6**] = 10:1) vesicular solution dramatically disappeared after adjusting the solution pH to 5.0, and meanwhile no vesicle could be found by TEM any more (Figure 2c), due to the precipitation of **WP6** as acid form out of the acidic aqueous solution. And then water-soluble calcein as a model hydrophilic dye was successfully loaded into the **WP6** ⊃ **G** vesicles at pH = 7.4, where the calcein-loaded vesicles showed much larger size in morphology (for details, see Figure S7, Supporting Information). Subsequently, the release behavior of calcein-encapsulated supramolecular vesicles under acidic conditions was investigated. As expected, when the solution pH was adjusted to acidity, the release of calcein from the cavities of vesicles was obviously observed accompanied by the increase of fluorescence intensity of calcein (Figure S8, Supporting Information). All the above results clearly demonstrated that such **WP6** ⊃ **G** supramolecular vesicles exhibited a good pH-responsiveness, which endows them with the ability to encapsulate substrates at neutral condition and release them in response to an acidic condition.

Besides the pH-responsiveness, more importantly, these obtained **WP6** ⊃ **G** supramolecular vesicles have the capability of responding to Ca^{2+} due to the Ca^{2+}-induced vesicle fusion. On the basis of the TEM experiments, it was found that when $CaCl_2$ solution (5 mM) was added into the **WP6** ⊃ **G** vesicular solution where vesicles were formed with average diameters about 190 nm, the vesicle fusion process was observed with the large numbers of giant and irregular vesicles of almost 10-fold increase in the average diameter (~1−4 μm) (Figure 2d−f). Moreover, DLS results also demonstrated that the average diameters of vesicles increased sharply with the time extension during the fusion process and the size distribution of the vesicular solution became polydisperse after fusion (Figure S12,

Supporting Information), which were in good agreement with the TEM images. Subsequently, binary mixing assays using the Cetyl Rhodamine B (CERB) probe[13] was carried out to further verify the fusion process of **WP6 ⊃ G** vesicles upon addition of Ca^{2+}, which were recorded by confocal laser scanning microscope (Figure 3). With the addition of Ca^{2+} and the
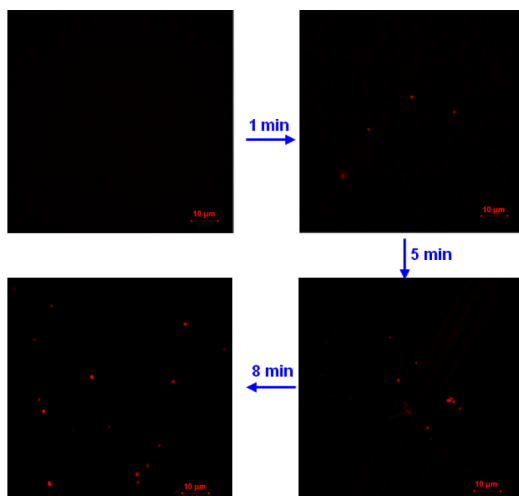
Figure 3. Images of vesicle fusion process obtained by confocal laser scanning fluorescence microscopy after the addition of calcium chloride (5.0 mM) from 0 to 8 min.

time extension, the fluorescence intensity of CERB gradually increased, but it terminated after 8 min, indicating the fast fusion process was completed within a very short period. Therefore, on the basis of the above observations together with the strong binding between **WP6** and Ca^{2+} ($(1.56 \pm 0.103) \times 10^4$ M^{-1}) confirmed by ITC experiments (Figure S11, Supporting Information), the **WP6 ⊃ G** vesicle fusion process should be dissected into the following three well-defined processes: first, Ca^{2+} binding to the carboxylate headgroups of **WP6**, which exist in the outside surface of the **WP6 ⊃ G** vesicles; then, such Ca^{2+}-**WP6** binding further induced the vesicle aggregation; and ultimately, merging of the bilayers resulted in the vesicle fusion.[8]

Since vesicle fusion process is accompanied by the release of the entrapped substrates, to further investigate the effect of Ca^{2+} concentration on the vesicle fusion process, after the above supramolecular vesicles were loaded with calcein, a different amount of Ca^{2+} was added and then calcein-release caused by vesicle fusion was monitored by fluorescence measurement (Figure 4). It was found that with the increase of Ca^{2+} concentration that was added, the releasing percentage of calcein gradually increased. While when the concentration of Ca^{2+} was increased to 10 mM, the releasing rate obviously reduced, and then flocculation of the fused aggregated became a dominant process. Therefore, based on the above meaningful investigation, Ca^{2+}-induced rapid fusion process of supramolecular **WP6 ⊃ G** vesicles was demonstrated for the first time, which might provide some useful information for understanding the fusion process associated with noncovalent interactions and attract considerable attention in the field of biotechnology, diagnostics, and DDS.

In addition, it is well-known that the gel-to-liquid crystalline temperature of the SAINT molecules such as **G** in this case is around 30 °C,[6c,10] which means that the alkyl chains of **G** are
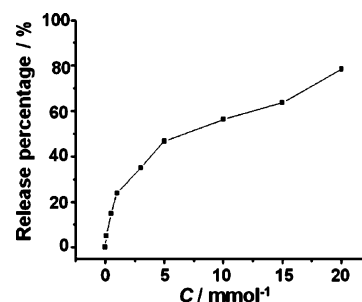
Figure 4. Calcium-induced calcein-loaded vesicle fusion led to the release of calcein in the presence of different Ca^{2+} concentrations that was added.

fully extended and ordered with the temperature below 30 °C, but such ordered structure will "melt" to liquid-like arrangement with the temperature above 30 °C.[1a,10a,14] Therefore, the **WP6 ⊃ G** supramolecular vesicles might exhibit a thermal-responsiveness. It was found that the standard **WP6 ⊃ G** vesicular solution was transparent with a light blue opalescence at 20 °C (Figure 5a); however, after it was heated at 36 °C for 5
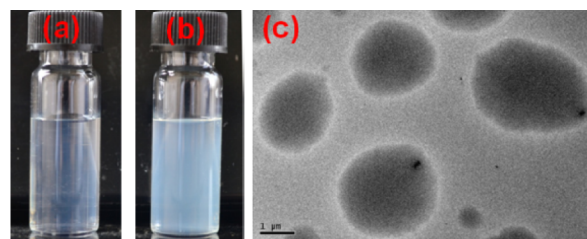
Figure 5. WP6 + G vesicular solution ([**WP6**] = 1.7×10^{-5} M, [**G**] = 1.46×10^{-4} M): (a) at 20 °C; (b) at 36 °C for 5 min; (c) TEM images of **WP6 + G** vesicular solution after standing at 36 °C for 5 min.

min, which is above the gel-to-liquid crystalline temperature, the vesicular solution became remarkably cloudy and its turbidity sharply increased (Figure 5b). Meanwhile, the DLS experimental result suggested that the average diameter of the vesicles became much larger after heating than before heating (Figure S9, Supporting Information). More intuitively, its TEM images showed that the newly generated giant vesicles (1−3 μm) were observed after heating at 36 °C for 5 min (Figure 5c), which was attributed to the thermal-induced fusion of small vesicles, indicating the thermal-responsiveness of **WP6 ⊃ G** vesicles. This temperature-dependent vesicle fusion effect was similar to previously reported interdigitation-fusion vesicles (IFVs),[1c,15] which also possessed a very large captured volume. Especially, ζ-potential of such obtained giant vesicles was about −40 mv (Figure S10a, Supporting Information), and no calcein release could be observed from such calcein-encapsulated giant vesicles based on the fluorescence detection even after standing at water bath (37 °C) for 48 h (Figure S10b, Supporting Information), indicating the high stability of such obtained giant vesicles. To the best of our knowledge, in the previous study helper lipid or cholesterol was often used to enhance the stability of vesicles formed from SAINT molecules,[1a,7a,8f,16] whereas the enhanced stability of the above supramolecular giant vesicles formed from **WP6 ⊃ G** was probably attributed to the presence of cooperative noncovalent interactions. These giant vesicles with large internal volume and good stability might be particularly attractive for biomimetic and bioimaging applications.

Encapsulation of Hydrophobic Drug Doxorubicin by Vesicles and its Multiresponsive Release. The obtained pH- and Ca^{2+}-responvsive **WP6 ⊃ G** supramolecular vesicles could be "smart" for controlled drug release. Herein, doxorubicin (DOX), one kind of hydrophobic anticancer drug and a fluorescence dye, was used to investigate the DOX encapsulation efficiency of the **WP6 ⊃ G** vesicles as well as its release behavior by external stimuli. After being desalted by TEA, DOX could be successfully loaded in the hydrophobic Stern layer of the vesicles, and the unloaded DOX was removed by dialysis against water. As is shown in Figure 6b, the UV
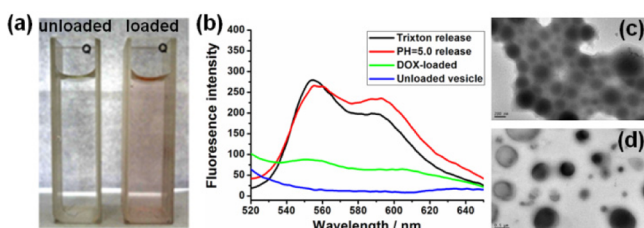
Figure 6. (a) Color changes of DOX-loaded vesicle (right) compared with unloaded one (left). (b) Fluorescence emission spectra of DOX-loaded vesicles in water (pH = 7.4), DOX-loaded vesicles when pH = 5.0 at 25 °C, and DOX-loaded vesicles treated with Trixton-100 (λ_{ex} = 484.0 nm). (c−d) TEM images of DOX-loaded vesicles in water under different measurement scale.

absorption of DOX-loaded vesicular solution from 530 to 600 nm became much stronger than the unloaded vesicles, which represents the characteristic absorption of DOX in aqueous solution. More intuitively, the vesicular solution turned from colorless to light pink after DOX was successfully loaded (Figure 6a). Meanwhile, TEM images showed that DOX-loaded vesicles were much larger in size than those of the unloaded vesicles (Figure 6c,d), further confirming the loading of DOX into the vesicles. On the basis of the fluorescence spectra, the DOX encapsulation efficiency was calculated to be 5.2%, indicating that such supramolecular vesicle was a good hydrophobic-drug-loading system. Subsequently, the release behavior of DOX-loaded supramolecular vesicles was investigated at pH 3.5, 5.0, and 7.4, respectively, and the release profiles were recorded as shown in Figure 7a. The results indicated that a gradual release of DOX was observed under acidic conditions (pH 5.0 or pH 3.5), with the cumulative release amount of 37% at pH 5.0 and 50% at pH 3.5, respectively, in the first 5 h. However, the cumulative leakage of DOX was less than 5% within 5 h under the physiological conditions (pH 7.4). Since the microenvironment of tumor
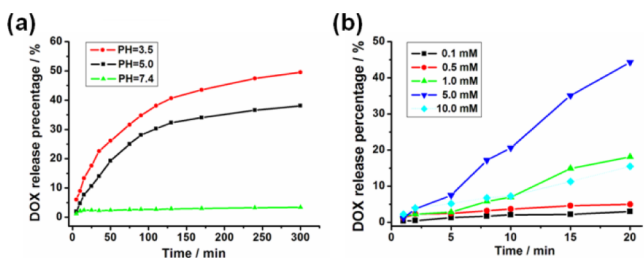
tissue is acidic due to the presence of excessive lactic acid and CO_2 as metabolites,[17] the release of DOX from DOX-loaded vesicles could be suspended in normal cells lease profiles, it was also found that this pH-responsive DOX release behavior was a slow process under acidic conditions, which, thus, could prolong the administering time and decrease the effect of toxicity.[18]

More importantly, when a different amount of $CaCl_2$ was added to the DOX-loaded vesicular solution, Ca^{2+}-induced vesicle fusion accompanied by a rapid release of encapsulated DOX could be observed (Figure 7b), where fluorescence spectroscopy was used to monitor the release efficiency of DOX upon addition of a different amount of Ca^{2+}. As shown in Figure 7b, the persence of Ca^{2+} from 0.1 to 5.0 mM that was added triggered a gradual enhancement of DOX release from 3% to 43% in the first 20 min However, when the concentration of Ca^{2+} was increased to 10 mM, only 15% of DOX was released under this condition. This is the reason that the fused vesicles started flocculating at higher concentration of Ca^{2+}, and then more and more released DOX was adhered into the resulting precipitates, due to the fact that DOX is a hydrophobic drug and was loaded in the hydrophobic Stern layer of the vesicles. Since Ca^{2+} plays essential roles in a number of biochemical processes, such Ca^{2+}-responsive fusion-releasing behavior of this **WP6 ⊃ G** supramolecular vesicle system will be considerably attractive in the field of biotechnology, diagnostics, and DDS.[9e,19]

Cytotoxicity and Anticancer Efficiency of DOX-Loaded Vesicles. To further investigate the cytotoxicity of the **WP6 ⊃ G** vesicles and the anticancer efficiency of DOX-loaded vesicles with the controlled release of DOX, MTT assay was then performed. Initially, unloaded vesicles, DOX, and DOX-loaded vesicles were incubated with NIH3T3 cells (normal cells), respectively, and the relative cell viability in different groups was recorded from 24 to 96 h. As shown in Figure 8a, the relative cell viability incubated with the unloaded
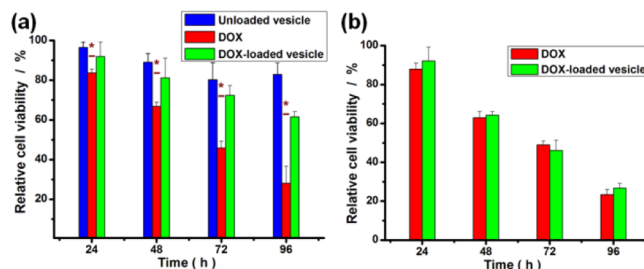
Figure 8. (a) Effects of unloaded vesicles, DOX, and DOX-loaded vesicles on viability of NIH3T3 cells at different time. (b) Anticancer activity of free DOX and DOX-loaded vesicles in MCF-7 cells at different time. Statistically significant differences were observed ($p < 0.05$) (*).

Figure 7. (a) pH-Responsive DOX release profiles of the DOX-loaded vesicles in the release media of different pH values. (b) Ca^{2+}-induced DOX-loaded vesicle fusion accompanied by DOX release in the presence of different Ca^{2+} concentration that was added.

vesicle group and the DOX-loaded vesicle group were both much higher than that in the DOX group from 24 to 96 h ($P < 0.05$), undoubtedly indicating that the low cytotoxicity of the unloaded and the DOX-loaded vesicles. Moreover, from the morphology of living cells we could also found that cells incubated with the DOX-loaded vesicle group were better than that in the DOX group even after 96 h (Figure 9c,d), indicating that the systemic toxicity of DOX was greatly reduced upon its encapsulation by **WP6 ⊃ G** vesicles. Subsequently, the relative viability of MCF-7 cells (cancer cells) incubated with DOX and
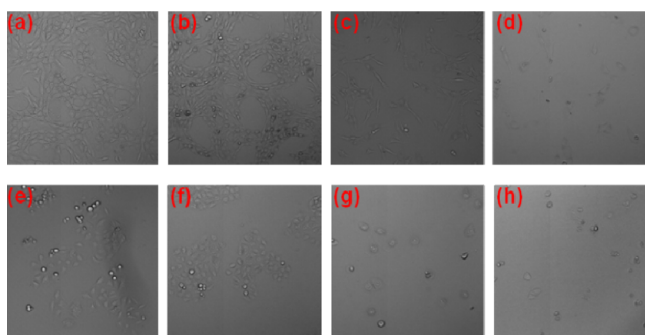
Figure 9. Images of living NIH3T3 cells in (a) blank, (b) blank vesicle, (c) DOX-loaded vesicle, and (d) DOX groups after 96 h. The images of living MCF7 cells in (e) blank, (f) blank vesicle, (g) DOX-loaded vesicle, and (h) DOX groups after 96 h.

DOX-loaded vesicles, respectively, was investigated. It was found that the relative cell viability (Figure 8b) and cell images of DOX-loaded vesicle group against cancer cells after 96 h (Figure 9g,h) showed similar therapeutic effects as the free DOX group. The above results indicated that the loading of DOX by **WP6 ⊃ G** vesicles reduced its cytotoxicity for normal cells but kept the therapeutic effect of DOX for cancer cells. Therefore, such **WP6 ⊃ G** supramolecular vesicles based on the host−guest complexation of **WP6** and SAINT derivatives are promising drug nanocarriers.

CONCLUSIONS

In conclusion, we have successfully constructed self-assembled nanoscale supramolecular binary vesicles based on the host−guest complexation of **WP6** and SAINT derivative **G**. Significantly, benefiting from the intrinsic advantages of supramolecular interaction, the obtained **WP6 ⊃ G** vesicles showed pH-, thermal-, and Ca^{2+}-responsiveness. Adjusting the solution pH to the acidic condition could lead to the complete disruption of vesicles and resulted in the efficient release of the encapsulated substrates. More importantly, the introduction of Ca^{2+} could lead to the fast vesicle fusion and accompanied by the efficiently release of the entrapped substrates. In addition, increasing temperature of the vesicular solution led to the generation of giant vesicles with large internal volume and good stability, which might be particularly attractive for biomimetic and bioimaging applications. Drug loading and release experiments demonstrated that DOX could be successfully encapsulated by the vesicles, and the resulting DOX-loaded vesicles exhibited excellent pH- and Ca^{2+}-responsiveness for the controlled release of DOX. Finally, cell experiments showed that the loading of DOX by **WP6 ⊃ G** supramolecular vesicles did not affect the therapeutic effect of DOX for cancer cells, whereas its cytotoxicity for normal cells was remarkably reduced. The present study provides a novel method for the construction of multistimuli-responsive supramolecular nanocarriers, which have great potential applications for the drug delivery.

EXPERIMENTAL SECTION

Materials Preparation. Doxorubicin (DOX) (>98%) was provided by Melone Pharmaceutical Co., Ltd. (Dalian, China). **WP6**, **G**, **G′**, and CERB probe were synthesized and purified according to previously reported procedures, and they were identified by ^1H NMR spectroscopy, performed on a Bruker Advance DMX 300 MHz spectrometer, and mass spectrometry, performed on Finnigan Mat TSQ 7000 instruments.

ζ-Potential Measurement. ζ-potential measurement was performed at 20 °C on a Zeta sizer-Nano Z (Malvern Instruments, Ltd., Worcestershire, U.K.) using the Smoluchowski model for the calculation of the ζ-potential from the measured electrophoretic mobility.

DOX Loading and Release of WP6 ⊃ G Vesicles. DOX-loaded vesicles were prepared as follows: a certain amount of DOX was added to a solution containing **WP6** and **G** (4% EtOH was added to improve the solubility of **G**). The ultimate concentrations of DOX, **G**, and **WP6** were 0.168, 0.16, and 0.024 mM, respectively. After standing overnight, the prepared DOX-loaded vesicles were purified by dialysis (molecular weight cutoff 10 000) in distilled water for several times until the water outside the dialysis tube exhibited negligible DOX fluorescence.

The DOX encapsulation efficiency was calculated by the following equation.

$$\text{encapsulation efficiency } (\%) = (m_{\text{DOX-loaded}}/m_{\text{DOX}}) \times 100$$

where $m_{\text{DOX-loaded}}$ and m_{DOX} are mass of DOX encapsulated in vesicles and mass of DOX added, respectively. The mass of DOX was measured by a fluorescence spectrophotometer at 560 nm and calculated as relative to a standard calibration curve in the concentrations from 1.0 to 10.5 μg/mL in water.

0.05 M tris-HCl buffer solutions (pH = 7.4) and 0.1 M citrate buffer solutions (pH = 5.0) were used as drug release media to simulate normal physiological conditions and the intracellular conditions of tumor. In a typical release experiment, 8.4 mL of DOX-loaded vesicles was added into 1.6 mL of appropriate release medium at 37 °C. At selected time intervals, 2 mL of the release media was taken out for measuring the released DOX concentrations by the fluorescence technique, and then was returned to the original release media. The concentration of DOX was determined by measurement of emission intensity at 560 nm using a standard emission vs concentration curve constructed for DOX in the corresponding release buffer. With the addition of Triton X-100 to the vesicle solution, a nearly 100% release of DOX from DOX-loaded vesicles could be obtained.

In a typical Ca^{2+}-induced release experiment, a certain amount of $CaCl_2$ solution was added into 15 mL of DOX-loaded vesicular solution, the final Ca^{2+} concentration was 0.1 mM, 0.5 mM, 1 mM, 5 mM, and 10 mM, respectively in the vesicular solution. At selected time intervals, 2 mL of the release media was taken out for measuring the released DOX concentrations by the fluorescence technique, and then was returned to the original release media. The concentration of DOX was determined by measurement of emission intensity at 560 nm using a standard emission vs concentration curve constructed for DOX in the corresponding release medium. A nearly 100% release of DOX from DOX-loaded vesicles could be obtained by adding Triton X-100 to the vesicular solution.

UV−Vis Absorption and Fluorescence Emission Spectra. UV−vis spectra were recorded in a quartz cell (light path 10 mm) on a PerkinElmer Lambda 35 UV/vis Spectrometer. Steady-state fluorescence spectra were recorded in a conventional quartz cell (light path 10 mm) on a PerkinElmer LS55 Fluorescence Spectrometer.

Transmission Electron Microscopy (TEM), Dynamic Light Scattering (DLS), and Confocal Laser Scanning Experiments. TEM images were recorded on a JEM-2100 instrument. The sample for TEM measurements was prepared by dropping the solution onto a carbon-coated copper grid. DLS measurements were performed under a Brookhaven BI-9000AT system (Brookhaven Instruments Corporation, USA) equipped with a 200 mW laser light and operating at λ = 514 nm. Confocal laser scanning images were taken by LSM 710 system (Zeiss Instruments Corporation, Germany).

Isothermal Microcalorimetric Titration. All calorimetric experiments were performed using a thermostated and fully computer operated ITC-200 calorimeter purchased from GE Instruments Corporation. In this study, the microcalorimetric titrations were performed in a D.I solution at atmospheric pressure. Each solution was degassed and thermostated before titration. Each microcalorimetric titration experiment consisted of 35 or 29 successive injections. A constant volume (1.1 μL/injection to **G′** or 1.3 μL/injection to **G**) of

WP6 solution (0.1−2 mM for each host) in a 40 μL syringe was injected into the reaction cell (200 μL) charged with **G'** or **G** solution (0.01−0.2 mM) in the same solution.

A control experiment to determine the heat of dilution was carried out with each run by performing the same number of injections with the same concentration of host compound as used in the titration experiments into a deionized water solution without the guest compound. The dilution enthalpies determined in control experiments were subtracted from the enthalpies measured in the titration experiments to obtain the net reaction heat.

ORIGIN software, which was used to simultaneously compute the equilibrium constant (K_a) and standard molar enthalpy of reaction ($\Delta H°$) from a single titration curve, gave a standard deviation based on the scatter of the data points in the titration curve. The net reaction heat in each run was calculated by the "one set of binding sites" model unless noted otherwise. Additionally, the first point was removed from the titration curve, acknowledging that the concentration of guest in the cell far exceeded the concentration of the host. The knowledge of the binding constant (K_a) and molar reaction enthalpy ($\Delta H°$) enabled calculation of entropy changes ($\Delta S°$), according to the equation where R is the gas constant and T is the absolute temperature. A typical titration curve and the fitted results for the complexation of **WP6** with **G** or **G'** are shown in Figure S5 and S6 (Supporting Information), respectively.

In Vitro Cell Assay. MCF-7 cancer cells and NIH3T3 normal cells were cultivated, respectively in DMEM (Dulbecco's modified Eagle's medium) supplied with 10% FBS (fetal bovine serum) and antibiotics (50 U/mL of penicillin and 50/U mL of streptomycin) at 37 °C in a humidified atmosphere containing 5% CO_2.

The relative cytotoxicities of unloaded vesicles, DOX, and DOX-loaded vesicles against NIH3T3 normal cells and MCF-7 cancer cells were evaluated in vitro by Methylthiazol tetrazolium (MTT) assay. Briefly, the cells were seeded in 96-well plates at a density of 10^4 cells per well in 200 μL complete DMEM containing 10% fetal bovine serum, supplemented with 50 U/mL of penicillin and 50 U/mL of streptomycin, and cultured in 5% CO_2 at 37 °C for 24 h. Then NIH3T3 cells were incubated with unloaded vesicles, DOX, and DOX-loaded vesicles, respectively. MCF-7 cells were subsequently incubated with DOX and DOX-loaded vesicle, respectively. The ultimate concentrations of DOX, **WP6**, and **G** were 0.43, 1.2, and 8.0 μM, respectively. At the end of each incubation (24, 48, 72, or 96 h), the cells were washed and replenished with fresh culture medium, which were further incubated for 2 h. Subsequently, 20 μL of MTT solution was added into each cell and incubated for another 4 h. After that, the medium containing MTT was removed and dimethyl sulfoxide (DMSO, 100 μL) was added to each well to dissolve the MTT formazan crystals. Finally, the plates were shaken for 10 min, and the absorbance of formazan product was measured at 490 nm by a microplate reader (BioTek ELx808). Untreated cells in media were used as the blank control. All experiments were carried out with three replicates. The cytotoxicity was expressed as the percentage of the cell viability as compared with the blank control.

Statistical Analysis. Differences between treatment groups were statistically analyzed using the paired Student's t-test. A statistically significant difference was reported if $p < 0.05$ or less.

ASSOCIATED CONTENT

Ⓢ Supporting Information

Experimental procedures and supporting figures. This material is available free of charge via the Internet http://pubs.acs.org.

AUTHOR INFORMATION

Corresponding Author

lywang@nju.edu.cn

Author Contributions

∥Yu Cao and Xiao-Yu Hu contributed equally.

Notes

The authors declare no competing financial interest.

REFERENCES

(1) (a) Scarzello, M.; Chupin, V.; Wagenaar, A.; Stuart, M. C. A.; Engberts, J. B. F. N.; Hulst, R. *Biophys. J.* **2005**, *88*, 2104. (b) Jiao, D.; Geng, J.; Loh, X. J.; Das, D.; Lee, T.-C.; Scherman, O. A. *Angew. Chem., Int. Ed.* **2012**, *51*, 9633. (c) Ahl, P. L.; Chen, L.; Perkins, W. R.; Minchey, S. R.; Boni, L. T.; Taraschi, T. F.; Janoff, A. S. *Biochim. Biophys. Acta, Biomembr.* **1994**, *1195*, 237. (d) Menger, F. M.; Gabrielson, K. *J. Am. Chem. Soc.* **1994**, *116*, 1567. (e) Menger, F. M.; Seredyuk, V. A. *J. Am. Chem. Soc.* **2003**, *125*, 11800. (f) Dwars, T.; Paetzold, E.; Oehme, G. *Angew. Chem., Int. Ed.* **2005**, *44*, 7174. (g) Boussif, O.; Lezoualc'h, F.; Zanta, M. A.; Mergny, M. D.; Scherman, D.; Demeneix, B.; Behr, J. P. *Proc. Natl. Acad. Sci. U. S. A.* **1995**, *92*, 7297.

(2) For representative stimuli-responsive supramolecular vesicles, see: (a) Guo, D.-S.; Wang, K.; Wang, Y.-X.; Liu, Y. *J. Am. Chem. Soc.* **2012**, *134*, 10244. (b) Nalluri, S. K. M.; Voskuhl, J.; Bultema, J. B.; Boekema, E. J.; Ravoo, B. J. *Angew. Chem., Int. Ed.* **2011**, *50*, 9747. (c) Ta, T.; Convertine, A. J.; Reyes, C. R.; Stayton, P. S.; Porter, T. M. *Biomacromolecules* **2010**, *11*, 1915. (d) Duan, Q.; Cao, Y.; Li, Y.; Hu, X.; Xiao, T.; Lin, C.; Pan, Y.; Wang, L. *J. Am. Chem. Soc.* **2013**, *135*, 10542. (e) Yu, G.; Zhou, X.; Zhang, Z.; Han, C.; Mao, Z.; Gao, C.; Huang, F. *J. Am. Chem. Soc.* **2012**, *134*, 19489. (f) Yu, G.; Xue, M.; Zhang, Z.; Li, J.; Han, C.; Huang, F. *J. Am. Chem. Soc.* **2012**, *134*, 13248. (g) Yu, G.; Han, C.; Zhang, Z.; Chen, J.; Yan, X.; Zheng, B.; Liu, S.; Huang, F. *J. Am. Chem. Soc.* **2012**, *134*, 8711. (h) Lee, M.; Lee, S.-J.; Jiang, L.-H. *J. Am. Chem. Soc.* **2004**, *126*, 12724. (i) Wang, C.; Guo, Y.; Wang, Y.; Xu, H.; Zhang, X. *Chem. Commun.* **2009**, 5380. (j) Yao, Y.; Xue, M.; Chen, J.; Zhang, M.; Huang, F. *J. Am. Chem. Soc.* **2012**, *134*, 15712. (k) Saito, G.; Swanson, J. A.; Lee, K.-D. *Adv. Drug Delivery Rev.* **2003**, *55*, 199.

(3) (a) Wang, K.; Guo, D.-S.; Wang, X.; Liu, Y. *ACS Nano* **2011**, *5*, 2880. (b) Gao, L.; Zheng, B.; Yao, Y.; Huang, F. *Soft Matt.* **2013**, *9*, 7314.

(4) (a) Sun, Y.-L.; Yang, B.-J.; Zhang, S. X.-A.; Yang, Y.-W. *Chem.—Eur. J.* **2012**, *18*, 9212. (b) Sun, Y.-L.; Yang, Y.-W.; Chen, D.-X.; Wang, G.; Zhou, Y.; Wang, C.-Y.; Stoddart, J. F. *Small* **2013**, *9*, 3224.

(5) (a) Ogoshi, T.; Hashizume, M.; Yamagishi, T.-a.; Nakamoto, Y. *Chem. Commun.* **2010**, *46*, 3708. (b) Ma, Y.; Ji, X.; Xiang, F.; Chi, X.; Han, C.; He, J.; Abliz, Z.; Chen, W.; Huang, F. *Chem. Commun.* **2011**, *47*, 12340. (c) Li, C.; Ma, J.; Zhao, L.; Zhang, Y.; Yu, Y.; Shu, X.; Li, J.; Jia, X. *Chem. Commun.* **2013**, *49*, 1924.

(6) (a) Nusselder, J. J. H.; Engberts, J. B. F. N. *J. Org. Chem.* **1991**, *56*, 5522. (b) Fadnavis, N. W.; Engberts, J. B. F. N. *J. Org. Chem.* **1982**, *47*, 2923. (c) Sudhoelter, E. J. R.; Engberts, J. B. F. N.; Hoekstra, D. *J. Am. Chem. Soc.* **1980**, *102*, 2467.

(7) (a) van der Woude, I.; Wagenaar, A.; Meekel, A. A. P.; ter Beest, M. B. A.; Ruiters, M. H. J.; Engberts, J. B. F. N.; Hoekstra, D. *Proc. Natl. Acad. Sci. U. S. A.* **1997**, *94*, 1160. (b) Meekel, A. A. P.; Wagenaar, A.; Šmisterová, J.; Kroeze, J. E.; Haadsma, P.; Bosgraaf, B.; Stuart, M. C. A.; Brisson, A.; Ruiters, M. H. J.; Hoekstra, D.; Engberts, J. B. F. N. *Eur. J. Org. Chem.* **2000**, 665. (c) Roosjen, A.; Šmisterová, J.; Driessen, C.; Anders, J. T.; Wagenaar, A.; Hoekstra, D.; Hulst, R.; Engberts, J. B. F. N. *Eur. J. Org. Chem.* **2002**, 1271. (d) Hulst, R.; Muizebelt, I.; Oosting, P.; van der Pol, C.; Wagenaar, A.; Šmisterová, J.; Bulten, E.; Driessen, C.; Hoekstra, D.; Engberts, J. B. F. N. *Eur. J. Org. Chem.* **2004**, 835. (e) Šmisterová, J.; Wagenaar, A.; Stuart, M. C. A.; Polushkin, E.; ten Brinke, G.; Hulst, R.; Engberts, J. B. F. N.; Hoekstra, D. *J. Biol. Chem.* **2001**, *276*, 47615.

10768

dx.doi.org/10.1021/ja505344t | *J. Am. Chem. Soc.* 2014, 136, 10762−10769

(8) (a) Duzgunes, N.; Straubinger, R. M.; Baldwin, P. A.; Friend, D. S.; Papahadjopoulos, D. *Biochemistry* **1985**, *24*, 3091. (b) Zhou, Y.; Yan, D. *Angew. Chem., Int. Ed.* **2005**, *44*, 3223. (c) Ravoo, B. J.; Kevelam, J.; Weringa, W. D.; Engberts, J. B. F. N. *J. Phys. Chem. B* **1998**, *102*, 11001. (d) Zhou, Y.; Yan, D. *J. Am. Chem. Soc.* **2005**, *127*, 10468. (e) Ellens, H.; Bentz, J.; Szoka, F. C. *Biochemistry* **1985**, *24*, 3099. (f) Ravoo, B. J.; Engberts, J. B. F. N. *J. Chem. Soc., Perkin Trans. 2* **2001**, 1869. (g) Menger, F. M.; Angelova, M. I. *Acc. Chem. Res.* **1998**, *31*, 789. (h) Bentz, J.; Duezguenes, N. *Biochemistry* **1985**, *24*, 5436. (i) Duzgunes, N.; Paiement, J.; Freeman, K. B.; Lopez-Straubinger, N. G.; Wilschut, J.; Papahadjopoulos, D. *Biochemistry* **1984**, *23*, 3486.

(9) (a) Newmark, H. L.; Wargovich, M. J.; Bruce, W. R. *J. Natl. Cancer Inst.* **1984**, *72*, 1323. (b) Durham, A. H.; Walton, J. *Biosci. Rep.* **1982**, *2*, 15. (c) Berridge, M. J.; Bootman, M. D.; Lipp, P. *Nature* **1998**, *395*, 645. (d) Bunn, P. A.; Dienhart, D. G.; Chan, D.; Puck, T. T.; Tagawa, M.; Jewett, P. B.; Braunschweiger, E. *Proc. Natl. Acad. Sci. U. S. A.* **1990**, *87*, 2162. (e) Monteith, G. R.; McAndrew, D.; Faddy, H. M.; Roberts-Thomson, S. J. *Nat. Rev. Cancer* **2007**, *7*, 519.

(10) (a) Kuiper, J. M.; Stuart, M. C. A.; Engberts, J. B. F. N. *Langmuir* **2007**, *24*, 426. (b) Scarzello, M.; Wagenaar, A.; Stuart, M. C. A.; Hoekstra, D.; Engberts, J. B. F. N.; Hulst, R. *J. Am. Chem. Soc.* **2005**, *127*, 10420.

(11) (a) Liu, Y.; Li, X.-Y.; Zhang, H.-Y.; Li, C.-J.; Ding, F. *J. Org. Chem.* **2007**, *72*, 3640. (b) Guo, D.-S.; Chen, S.; Qian, H.; Zhang, H.-Q.; Liu, Y. *Chem. Commun.* **2010**, *46*, 2620. (c) Guo, D.-S.; Wang, L.-H.; Liu, Y. *J. Org. Chem.* **2007**, *72*, 7775.

(12) Wiese, G. R.; Healy, T. W. *Trans. Faraday Soc.* **1970**, *66*, 490.

(13) (a) Sakagami, H.; Kamata, A.; Nishimura, H.; Kasahara, J.; Owada, Y.; Takeuchi, Y.; Watanabe, M.; Fukunaga, K.; Kondo, H. *Eur. J. Neurosci.* **2005**, *22*, 2697. (b) Ravoo, B. J.; Weringa, W. D.; Engberts, J. B. F. N. *Cell Biol. Int.* **2000**, *24*, 787. (c) Keller, P. M.; Person, S.; Snipes, W. *J. Cell. Sci.* **1977**, *28*, 167.

(14) (a) Tristram-Nagle, S.; Wiener, M. C.; Yang, C. P.; Nagle, J. F. *Biochemistry* **1987**, *26*, 4288. (b) Blandamer, M. J.; Briggs, B.; Cullis, P. M.; Engberts, J. B. F. N. *Chem. Soc. Rev.* **1995**, *24*, 251. (c) Blandamer, M. J.; Briggs, B.; Cullis, P. M.; Engberts, J. B. F. N.; Wagenaar, A.; Smits, E.; Hoekstra, D.; Kacperska, A. *J. Chem. Soc., Faraday Trans.* **1994**, *90*, 2709.

(15) Janoff, A. S.; Minchey, S. R.; Perkins, W. R.; Boni, L. T.; Seltzer, S. E.; Adams, D. F.; Blau, M. *Invest. Radiol.* **1991**, *26*, S167.

(16) (a) Sudhoelter, E. J. R.; De Grip, W. J.; Engberts, J. B. F. N. *J. Am. Chem. Soc.* **1982**, *104*, 1069. (b) Nusselder, J. J. H.; Engberts, J. B. F. N. *J. Am. Chem. Soc.* **1989**, *111*, 5000.

(17) (a) Danhier, F.; Feron, O.; Préat, V. *J. Controlled Release* **2010**, *148*, 135. (b) Fukumura, D.; Jain, R. K. *J. Cell. Biochem.* **2007**, *101*, 937. (c) Rofstad, E. K.; Mathiesen, B.; Kindem, K.; Galappathi, K. *Cancer Res.* **2006**, *66*, 6699. (d) Vaupel, P.; Kallinowski, F.; Okunieff, P. *Cancer Res.* **1989**, *49*, 6449.

(18) (a) Gabizon, A.; Catane, R.; Uziely, B.; Kaufman, B.; Safra, T.; Cohen, R.; Martin, F.; Huang, A.; Barenholz, Y. *Cancer Res.* **1994**, *54*, 987. (b) Allen, T. M.; Hansen, C.; Martin, F.; Redemann, C.; Yau-Young, A. *Biochim. Biophys. Acta, Biomembr.* **1991**, *1066*, 29. (c) Dash, A. K.; Cudworth, G. C. *J. Pharmacol. Toxicol. Methods* **1998**, *40*, 1.

(19) (a) Sethi, T.; Rozengurt, E. *Cancer Res.* **1991**, *51*, 1674. (b) Nygren, P.; Larsson, R.; Gruber, A.; Peterson, C.; Bergh, J. *Br. J. Cancer* **1991**, *64*, 1011. (c) Bergmann, J.; Junghahn, I.; Brachwitz, H.; Langen, P. *Anticancer Res.* **1994**, *14*, 1549. (d) Bergner, A.; Huber, R. M. *Anticancer Agents Med. Chem.* **2008**, *8*, 705.